UCRL-TR-225388

LAWRENCE
LIVERMORE
NATIONAL
LABORATORY

X-ray Diffraction Techniques for Structural Determination of Amorphous Materials

C. K. Saw, T. Lian, S. D. Day, J. C. Farmer

October 18, 2006

Disclaimer

X-ray Diffraction Techniques for Structural Determination of Amorphous Materials*.

C.K. Saw, T. Lian, S. D. Day and J. C. Farmer
Lawrence Livermore National Laboratory

I. SUMMARY

Prevention of corrosion is a vital goal for the Department of Defense when billions of dollars are spent every year. Corrosion resistant materials have applications in all sort of military vehicles, and more importantly in naval vessels and submarines which come in contact with the seawater. An important application of the corrosion resistant material is in the radioactive waste disposable field where the vessels or containers are expected to hold the radioactive toxic materials for thousands of years to surpass the half life of the radiation. It has been known that corrosion resistance can be improved by the used of structurally designed materials in the amorphous state where the atoms are arranged in a non-periodic conditions, even though, some local chemical short range ordering may occur in the amorphous arrangement. On the other hand, the final material can also be elementally tailored to specific application. This work documents in details the characterization effort for the amorphous materials using x-ray diffraction technique as part of the High Performance Corrosion-Resistant Material – Structural Amorphous Metal (HPCRM-SAM) program here at LLNL. The samples are in the form of powders, ribbons and coatings deposited onto parts. Some brief theoretical background is given in order to interpret the results, instrumentation will also be described. The results suggest that the formation of amorphous phase in the metal alloys powders greatly depends on the processing conditions. In most of the powders, especially lot #06, the result indicates that the materials are amorphous with a very small amount of iron boron alloy. In the ribbon samples, all the samples and of different compositions as well are observed to be amorphous. In most cases, starting from an amorphous powder sample, the coatings are also observed to be amorphous with a small amount of iron oxide, probably due to exposure to air during the thermal spraying process.

II. INTRODUCTION

Prevention of corrosion is a vital goal for the Department of Defense when billions of dollars are spent every year. Corrosion resistant materials have applications in all sort of military vehicles, and more importantly in naval vessels and submarines which come in contact with the seawater. It has been known [1] that corrosion resistance can be improved by the used of structurally designed materials in the amorphous state where the atoms are arranged in a non-periodic conditions. Corrosions in periodic condition are attributed to both the atomic structures as well as the microstructures. In the atomic structures, periodic tunnels exist whereby pathways occur where possibly ionic oxygen, nitrogen and hydrogen can travel through a crystal without significant obstructions. Loosely packed grain boundaries and often voids exist in crystalline materials which are susceptible to chemical attacks into the bulk of the materials, thus resulting in poor physical properties. Also, in crystalline structures, there exist anisotropic thermal expansions in the bulk by the nature of the periodic atomic arrangements and thus upon thermal cycling, the microstructures can be changed, resulting in possibly additional grain boundaries, dislocations and voids, which can initiate stress corrosion cracking.

In amorphous materials, also known as metallic glasses, atomic arrangements are essentially almost random where the precise atomic locations are not so critical, thermal expansion can now be highly isotropic, grain boundaries can be eliminated and as well as the presence of periodic tunnels. These behaviors essentially reduced stress corrosion cracking, thus increases the corrosion resistant property. Even though, local chemical short range order does occur in the amorphous arrangement but not in the long range order. Another advantage of using amorphous materials is that it can also be elementally tailored to specific application. Metallic glasses also often exhibit extraordinary mechanical and thermal properties, magnetic behavior and high corrosion resistance. These novel materials could be very important in the future of commercial and defense industries.

The present work focuses on the use of amorphous materials (powders) as a coating on parts to take advantage of the corrosion resistant property, thus protecting the parts which may be the skin of submarines and military vessels exposing to sea water or vessels for waste storage. Of interest to us is in the development of technology of using the thermal spraying the amorphous powders onto the surface of the objects, in this case, for the nuclear waste containers, by the high-velocity oxy-fuel (HVOF) process with no change in the structure. This report documents the characterization effort for the amorphous materials using x-ray diffraction technique in support of the HVOF program here at LLNL [2]. Some brief theoretical background is given in order to interpret the results, instrumentation will also be described and results be provided.

III. THEORETICAL CONSIDERATIONS

The basic theory of x-ray diffraction has been quite well covered in many text books [3]. For crystalline diffraction, specific x-ray peaks can be observed from a diffraction pattern

acquired from x-ray diffractometer for crystalline materials. These peaks are the results of constructive interference of the probing x-ray wave. If the sample is single crystal, these peaks have specific arrangements and orientations. The positions and intensities of these peaks are related to the atomic arrangements in the unit cell of the crystals. Unit cells have 3 axes with 3 angles (called lattice parameters) and they can be grouped into triclinic, monoclinic, orthorhombic, tetragonal, hexagonal, rhombohedral or cubic structures. In general, specific compounds have specific lattice parameters and the compounds can be identified by these parameters. The lattice parameters consist of three axes and three angles.

In an amorphous material, the atoms are not arranged in a periodic fashion such that crystals can be formed. The scattering intensity is then the summation of each individual atom. The time average scattering of non-interacting scattering like mono-atomic gases, the scattering is given by the Debye equation,

$$I_{eu} = \sum_m \sum_n f_m f_n \frac{\sin kr_{mn}}{kr_{mn}} \qquad (1)$$

f_m, f_n are the scattering factors, r_{mn} are the inter-atomic distances and k . This equation can be further reduced and converted to an integral,

$$I_{eu} = Nf^2 \left[1 + \int 4\pi\rho(r) \frac{\sin kr}{kr} dr \right] \qquad (2)$$

Using algebraic manipulation and defining $\rho(r) = [\rho(r) - \rho_o] + \rho_o$, this equation becomes

$$k[i(k)] = 4\pi \int_0^\infty r[\rho(r) - \rho_o] \sin kr dr \qquad (3)$$

where $i(k) = \dfrac{I_{eu}/N - f^2}{f^2}$, for simplicity and by using the theorem of Fourier's conversion, we can write the radial distribution function as

$$4\pi r^2 \rho(r) = 4\pi r^2 \rho_o + \frac{2r}{\pi} \int_0^\infty k[i(k)] \sin kr dk \qquad (4)$$

The above expression provided a mean of converting the intensity function, which is in k space (k=4to the radial distribution function in real space. In this formulation, the atoms are arranged in random fashion with no order. There are broad diffraction peaks, which belong to the amorphous structure. The amorphous state does have structure as defined by the radial distribution function and the partial radial distribution, if it is a multiple elements system [3]. For the present effort, such an analysis is not necessary at the moment.

In all, the degree of crystalline is correlated to the intensity of each scattering component.

IV. EXPERIMENTAL SETUPS

The X-ray diffraction experiment is carried out using the Philip vertical goniometer in the para-focusing or also known as the Bragg-Bretano method. The x-ray optics is shown in Figure 1. It is self-focusing and that is the distance between the x-ray focal point (F) to the sample position (A) is equal to the distance between the sample position (A) and the receiving slit (R) for the reflection mode. Thus, the intensity and resolution are optimized. Parallel vertical slits P and RP are also added to improve the scattering signal.
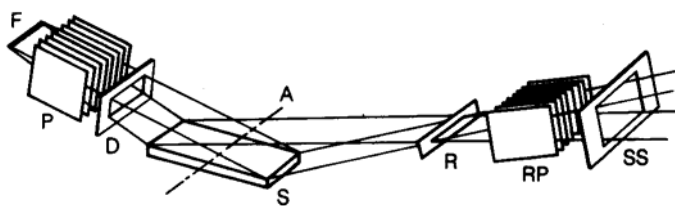

Figure 1: Para-focusing Bragg-Brentano geometry

In general, in most diffractometers scintillation detectors are used. However, the energy resolution is no sufficient to discriminate fluorescence x-rays of certain elements with energy close to the probing x-ray energy. Hence, very often, an analyzing crystal is used after the receiving slit. The choice of the crystal is based on the crystal mosaic, for energy selectivity and the efficiency. The most widely use energy discriminator is usually graphite for efficiency without significantly scarifying x-ray intensity. This is particularly important for the HPCRM because of the iron content in the samples. Iron fluorescence has energy which is close to that of the copper K_α probing x-ray. Sometime x-ray filters are used.

In the present setup, CuK_α is used with a graphite analyzing crystal. Step scan is performed from 20 to 90° (2θ) with step size of 0.02° at 4-10 seconds per point, depending on the amount of sample. The samples are loaded onto low quartz holders. This is because the expected intensity is very low and hence background scattering needs to be minimized.

V. SAMPLES

The samples are listed in the Tables I, II and III for powders, ribbons and coatings, respectively. They are also separated according to buckets in powders, presumably according to lot #'s and differences in processing conditions or also composition variations and particle sizes.

VI. RESULTS AND DISCUSSIONS

For clarity, the results can be divided into three groups according to the form that they are submitted, namely, powders, ribbons and coatings. The powders are as-prepared state, the

ribbons are essentially melt-spun from the powders and the coatings are thermal sprayed onto a surface.

VI (a) Powders

Figure 1 shows the resulting diffraction pattern for the SAM2X5 powder samples manufactured by The NanoSteel Company in 2004 and 2005. SAM2X5 is the Mo series with 5% Mo in SAM40 and SAM40 consists of 50Fe-18Cr-15B-2Si-2Mn-2W. The lot # and the powder fraction size are also given in the Table. Lot # 04 was produced in FY04, and lot #05 was produced in FY05. Particle sizes are listed along with the lot #'s. Lot # 05-079-53+15 means powder from lot # 05-079 with particle size ranging from 15 to 53 um. Both amorphous and crystalline phases can be observed. The results suggest that lot # 05 is more crystalline than lot # 04. Figure 2 compares the XRD patterns with some possible ICDD (International Center for Diffraction Data) data base compounds. It is most likely that the crystalline components are alloys of boron chromium, chromium carbide, possibly iron chromium and iron. An amorphous structure is observed for the lot #04-195-15 sample and partially amorphous for lot #04-199-30 and #04-200-53.

Figure 3 shows the resulting diffraction of the SAM2X5 powder from lot # 06-015 prepared in FY06, also labeled as "new" and lot # 05-263 labeled as "old" prepared in FY05 by Nanosteel. Clearly, they are not similar. Lot #06-015 is essentially amorphous. The crystalline lines appear to be those of alloys of iron carbide, boron iron and possible iron chromium as indicated in Figure 4.

Figures 5, 6 and 7 show the resulting diffraction patterns for a set of powder samples of SAM2X5 from lot #06-015 taken from different buckets labeled from 1 to 35. The results suggest, except for bucket #1, the powders are essentially similar with the major component having the amorphous structure and some amount of crystallinity. The small amount of crystallinity can probably be attributed to alloys of boron iron as indicated in Figure 8.

Figure 9 shows the diffraction patterns from the powders of lot #06-123. The results are very similar for all the samples from different bucket. Again, the major component is amorphous with minor crystalline phase which is probably alloy of boron iron as indicated in the ICDD listing of Figure 8.

VI (b) Ribbons

Melt-spun ribbons are also submitted for investigation. The samples were also prepared by NanoSteel Company. Figure 10 shows the resulting diffraction patterns of the melt spun ribbons for C22 and 316L steel which clearly indicate both materials are crystalline and melt spin process cannot capture the amorphous meta-stable state of these alloys.

Figure 11 compares the resulting diffraction pattern of ribbons for samples (a) SAM2X1, (b) SAM2X3, (c) SAM2X5 and (d) SAM2X7 for the Mo series where (a) is 1%, (b) 3%, (c) 5% and (d) 7% Mo concentration. Clearly, the results indicate that these ribbon samples are amorphous as evidence by a single broad x-ray peak.

Figure 12 shows the resulting diffraction pattern for (e) SAM6, (f) SAM7, (g) SAM8 and (h) SAM40 ribbons. Only one major broad peak is observed in all the samples indicating that the materials are amorphous. Figure 13 compares the diffraction patterns for the SAM1Xn series, where n is equals to 1, 3, 5 and 7 % nickel. The results indicate that the samples are amorphous and show no significant amount of crystallinity. Figure 14 compares the resulting diffraction patterns for the SAM3Xn series, where n is equals to 1, 3, 5 and 7% yttrium. Again, all the ribbons are essentially amorphous.

VI (c) Coatings

Figures 15-17 show all the coatings from SAM2X5 materials except one from SAM1651 as identified in 15 (b). Figure 15 shows the result for a set of coating samples where (a) E316L471 is a spalled coating of SAM1651 (b) E316L463 is the coating on a 316L substrate (c) E316L504 and (d) W316L329 are coatings on 316L substrate. In most cases, some level of crystallinity is observed on top of the major amorphous component. The spalled sample (a) and sample (c) SAM2X5 EL316L504 show the most amount of amorphous component. There are some crystalline lines and they can be indexed to iron oxide Fe_3O_4 as indicated in Figure 16.

Samples (b) 04-E316L471 and (d) 04-E316L504 are essentially similar. The major amorphous component can be observed with a small amount of crystallinity which is probably due to iron boron alloy and iron oxide as shown in Figure 17. For sample (f) M6SI lot #05-079, an additional crystalline component can be observed as indicated by the additional x-ray lines. The lines can be indexed to crystalline iron.

Figure 18 shows the diffraction patterns of alloy coatings, PTI-A, PTI-B and PTI-C on 316L substrate. Essentially, the material is amorphous, however some amount of crystalline component can be observed. The crystalline components are due to iron oxide and boron iron alloy. The resulting diffraction patterns for coatings from SAM2X5 lot # 06-015 labeled as PTI-358-C1, C2 and C3 are similar to that of PTI-C as shown in Figure 18. They are essentially amorphous with a small amount of crystallinity, probably due to iron oxide and iron boron.

VII. CONCLUSIONS

X-ray diffraction technique has been developed to examine the structure of SAM samples in the form of powder, ribbons and coatings. Since the samples contain a significant amount of iron, diffracted beam discrimination is needed. The results are consistent with those examined by other laboratory. From this work, it can be concluded that the production of amorphous iron base alloys material critically depends on the multiple elemental compositions. C22 and 316L alloys did not form the amorphous phase. The multiple elements essentially ensure the increase of the free energy, thus preventing like elements from forming crystalline ordered states.

Differences in crystallinity can be observed from the same powder samples of different lot's as evidence from the examination of the same materials. Both lot #05-079-53 and 05-

193-53 samples and lot #04 200-53 are highly crystalline which are identified to be alloys of boron chromium, chromium carbide, iron chromium, iron carbide and boron iron. Lot #04-199-30 is essentially amorphous. No processing information is available hence presumably these differences are due to thermal history and/or crystallite sizes. A new lot #06-015 powder sample was submitted and compared to the lot #05-063 and the result indicates that this new sample is amorphous. A set of powder samples of SAM2X5 of lot #06-015 from bucket #1 to #35 were examined. Except for sample from bucket #1 in lot #06-015 which has significantly more crystallinity, the major component is essentially amorphous for the rest of the samples with a very small amount of crystalline boron iron alloy. Lot #06-123 is also amorphous with a small amount of crystalline boron iron alloy.

Amorphous melt-spun ribbon samples cannot be prepared for C22 and 316L materials, they both show crystallinity. All the ribbons samples exhibit an amorphous structure. There are some differences in the structure of the thermal spray coatings depending on the starting powder samples. In most cases, the major amorphous component can be observed with a small amount of crystalline component. However, starting from an amorphous powder, an amorphous coating can be achieved with a small amount of crystallinity due to oxidation of iron.

VIII. REFERENCES

[1] Latanison, R.M., Workshop on Amorphous Metals and Semiconductors, EPRI, May 12-18 (1985)

[2] J. C. Farmer, J. J. Haslam, F. Wong, X. Ji, S. D. Day, D. J. Branagan, M. C. Marshall, B. E. Meacham, E. J. Buffa, C. A. Blue, J. D. K. Rivard, M. B. Beardsley, D. T. Weaver, L. F. Aprigliano, L. Kohler, R. Bayles, E. J. Lemieux, T. M. Wolejsza, F. J. Martin, N. Yang, G. Lucadamo, J.H. Perepezko, K. Hilda!, L. Kaufman, A. H. Heuer, F. Ernst, G. M. Michal, H. Kahn, E. J. Lavernia, "High-Performance Corrosion-Resistant Materials: Iron-Based Amorphous-Metal Thermal-Spray Coatings", Am. Soc. of Mechanical Engineers", Pressure Vessels & Piping (PVP) Conf. July 2005

[3] Saw, C.K., "X-ray Scattering Techniques for Characterization Tools in the Life Sciences", Nanotechnologies for the Life Science, Edited by Challa Kumar, Wiley-VCH Verlag GmbH & Co., KGaA, Weinheim, 2006

[4] Saw C.K. and Schwarz, R.B., "Chemical short-range order in dense random-packed models", J. of the Less-Common Metals, 1988, 140, 385-393

Table I: Samples description for the powders

X-ray #	ID	Description	Form	Label
X3017	Bucket #1	SAM 2x5 lot# 05-079-53 + 15	P	Amorphous +crystalline
X3018	Bucket #30	SAM 2x5 lot # 05-193-53	P	Amorphous +crystalline
X3019	Bucket #40	SAM 2x5 lot # 04-200-53 + 30	P	Amorphous +crystalline
X3020	Bucket #45	SAM 2x5 lot # 04-199-30 + 15	P	Amorphous +crystalline
X3021	Bucket #60	SAM 2x5 lot # 04-191-15	P	Amorphous
X3069	Nanosteel	SAM2X5 lot # 06-015	P	Amorphous
X3080	Nanosteel	SAM2X5 lot # 05-263	P	Amorphous + crystalline
X3132	Nanosteel	SAM2X5 lot # 06-015 Bucket #1	P	Amorphous +crystalline
X3133	Nanosteel	SAM2X5 lo t# 06-015 Bucket #2	P	Amorphous
X3134	Nanosteel	SAM2X5 lot # 06-015 Bucket #3	P	Amorphous
X3135	Nanosteel	SAM2X5 lot # 06-015 Bucket #4	P	Amorphous
X3144	Nanosteel	SAM2X5 lot # 06-015 Bucket #7	P	Amorphous
X3112	Nanosteel	SAM 2X5 lot # 06-015 bucket PT#8	P	Amorphous
X3113	Nanosteel	SAM 2X5 lot # 06-015 bucket PT#11	P	Amorphous
X3114	Nanosteel	SAM 2X5 lot # 06-015 bucket PT# 13	P	Amorphous
X3115	Nanosteel	SAM 2X5 lot # 06-015 bucket PT#15	P	Amorphous
X3116	Nanosteel	SAM 2X5 lot # 06-015 bucket PT#18	P	Amorphous
X3145	Nanosteel	SAM2X5 lot # 06-015 Bucket #14	P	Amorphous
X3146	Nanosteel	SAM2X5 lot # 06-015 Bucket #21	P	Amorphous
X3147	Nanosteel	SAM2X5 lot # 06-015 Bucket #28	P	Amorphous
X3148	Nanosteel	SAM2X5 lot # 06-015 Bucket #35	P	Amorphous
X3139	Nanosteel	SAM2X5 lot # 06-123 bucket #7	P	Amorphous +crystalline
X3140	Nanosteel	SAM2X5 lot # 06-123 bucket #9	P	Amorphous
X3141	Nanosteel	SAM2X5 lot # 06-123 bucket #11	P	Amorphous
X3142	Nanosteel	SAM2X5 lot # 06-123 bucket #13	P	Amorphous
X3143	Nanosteel	SAM2X5 lot # 06-123 bucket #15	P	Amorphous

Table II: Sample description for the ribbons

X3233	SAM1X1	SAM1X1 series 1% Ni	R	Amorphous
X3234	SAM1X3	SAM1X3 series 3% Ni	R	Amorphous
X3235	SAM1X5	SAM1X5 series 5% Ni	R	Amorphous
X3236	SAM1X7	SAM1X7 series 7% Ni	R	Amorphous
X3237	SAM3X1	SAM3X1 series 1%Y	R	Amorphous
X3238	SAM3X3	SAM3X3 series 3%Y	R	Amorphous
X3239	SAM3X5	SAM3X5 series 5%Y	R	Amorphous
X3240	SAM3X7	SAM3X7 series 7%Y	R	Amorphous
X3214	SAM2X1	SAM2X1 series 1% Mo	R	Amorphous + crystalline
X3214	SAM2X3	SAM2X3 series 3% Mo	R	Amorphous + crystalline
X3074	SAM2X5	SAM2X5 series 5% Mo	R	Amorphous
X3075	SAM2X7	SAM2X7 series 7% Mo	R	Amorphous
X3070	C22	57Ni-22Cr-13Mo-2Fe-3W-Co	R	Crystalline est. a=3.60A
X3071	316L	Fe-20Cr-10Ni-3Mo-Mn	R	Crystalline est. a=358A
X3076	SAM6	43Fe-16Cr-16Mo-10C-10P-5B	R	Amorphous
X3101	SAM7	Fe-Cr-Mo-B-C (1651)	R	Amorphous
X3102	SAM8	Fe-Cr-Mo-B-C (3%W)	R	Amorphous
X3079	SAM40	52Fe-19Cr-16B-4C-2Si-2Mo-2Mn-2W	R	Amorphous

Table III: Sample description for the coatings

X-ray #	ID	Description	Forms	
X3103	PWD05-079	SAM2X5 –powder 50Fe18Cr15B4C5Mo2Si2Mn2W (lot # 05)	P	Amorphous +crystalline
X3104	E316L471	Spalled coating SAM1651disk (lot #04)	C	Amorphous +crystalline
X3105	E316L463	SAM2X5 coating disk (lot # 04)	C	Amorphous +crystalline
X3106	E316L504	SAM2X5 lot # 04-119 -30+15 μm	C	Amorphous +crystalline
X3107	W316L329	SAM2X5 lot # 04-200 -52+30 μm	C	Amorphous +crystalline
X3108	M6S1	SAM2X5 lot # 05-079 -53+15 μm	C	Amorphous +crystalline
X3136	PTI-A	SAM2X5 on 316L substrate	C	Amorphous +crystalline
X3137	PTI-B	SAM2X5 on 316L substrate	C	Amorphous +crystalline
X3138	PTI-C	SAM2X5 on 316L substrate	C	Amorphous +crystalline
X3101b	SAM7	Fe-Cr-Mo-B-C "not shinning side"	R	Amorphous
X3159	PTI-358-C1	SAM2X5 lot # 06-015 coating	C	Amorphous +crystalline
X3160	PTI-358-C2	SAM2X5 lot # 06-015 coating	C	Amorphous +crystalline
X3161	PTI-358-C3	SAM2X5 lot # 06-015 coating	C	Amorphous + crystalline
X3241	316L-W10	316L plate with SAM2X5 lot #06-015	C	Amorphous
X3242	C22-W22	C22 plate coating SAM2X5 lot #06-015	C	Amorphous

C22: Ni-Cr-Mo-Fe-W-Co
316L: Fe-Cr-Ni-Mo-Mn
SAM2X1: Fe-Cr-B-C-Mo-Si-Mn-W
SAM2X3: Fe-Cr-B-C-Mo-Si-Mn-W
SAM2X5: Fe-Cr-B-C-Mo-Si-Mn-W
SAM2X7: Fe-Cr-B-C-Mo-Si-Mn-W
SAM2X1-50Fe-18Cr-15B-4C-1Mo-2Si-2Mn-2W
SAM2X3-50Fe-18Cr-15B-4C-3Mo-2Si-2Mn-2W
SAM2X5-50Fe-18Cr-15B-4C-5Mo-2Si-2Mn-2W
SAM2X7-50Fe-18Cr-15B-4C-7Mo-2Si-2Mn-2W
SAM6 -43Fe-16Cr-16Mo-10C-10P-5B
SAM7 -48Fe-15Cr-15C-14Mo-6B-2Y
SAM8 -47Fe-15Cr-15C-13Mo-6B-3W-2Y
SAM40 - 52Fe-19Cr-16B-4C-2Si-2Mo-2Mn-2W

Figure 1: XRD patterns for SAM2X5, lot 5, bucket 1, 20 and lot 4 bucket 40, 45 and 60.
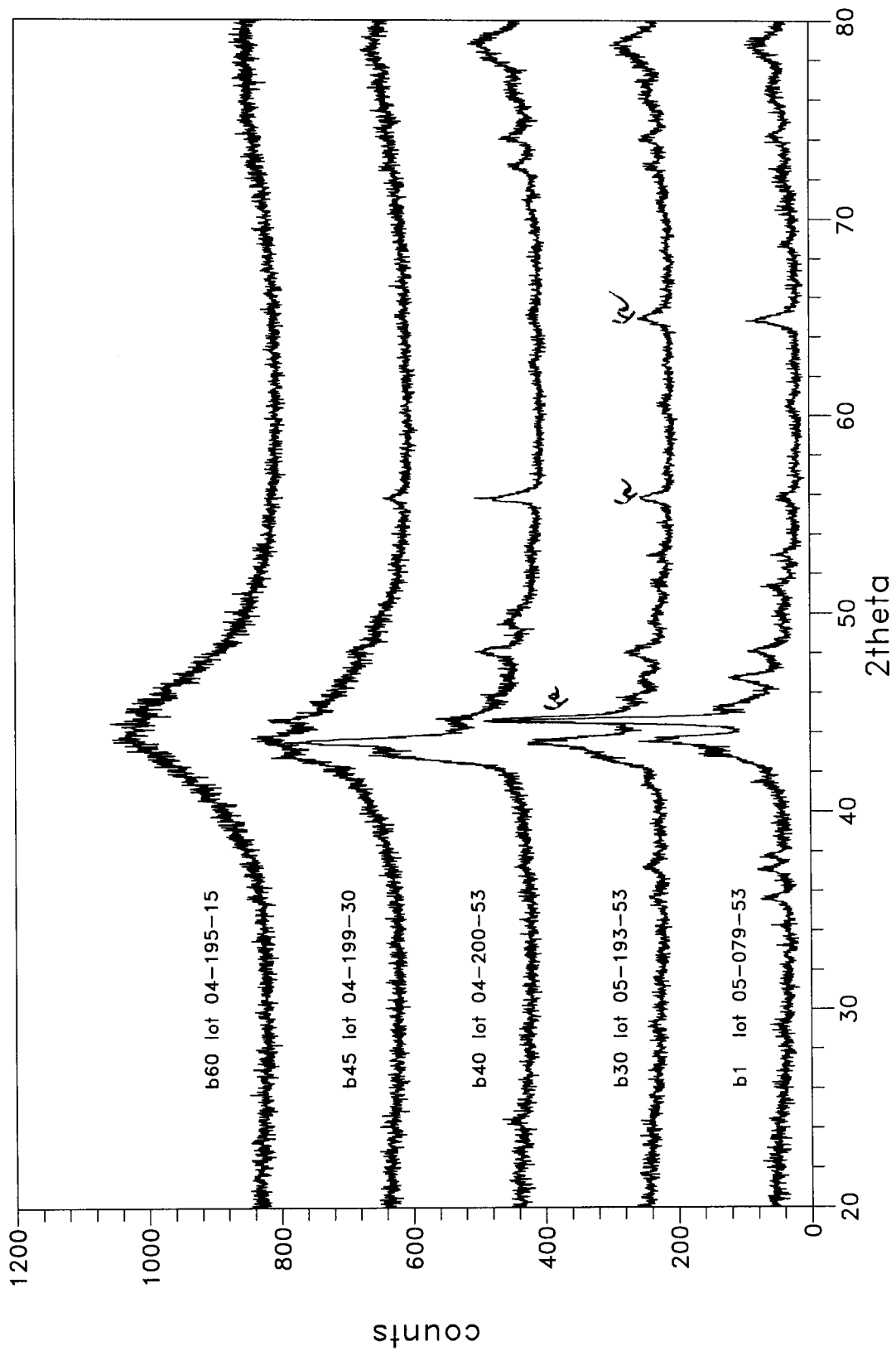
Figure 2: XRD patterns for SAM2X5 for bucket #1, #30 and #40 and ICDD listings
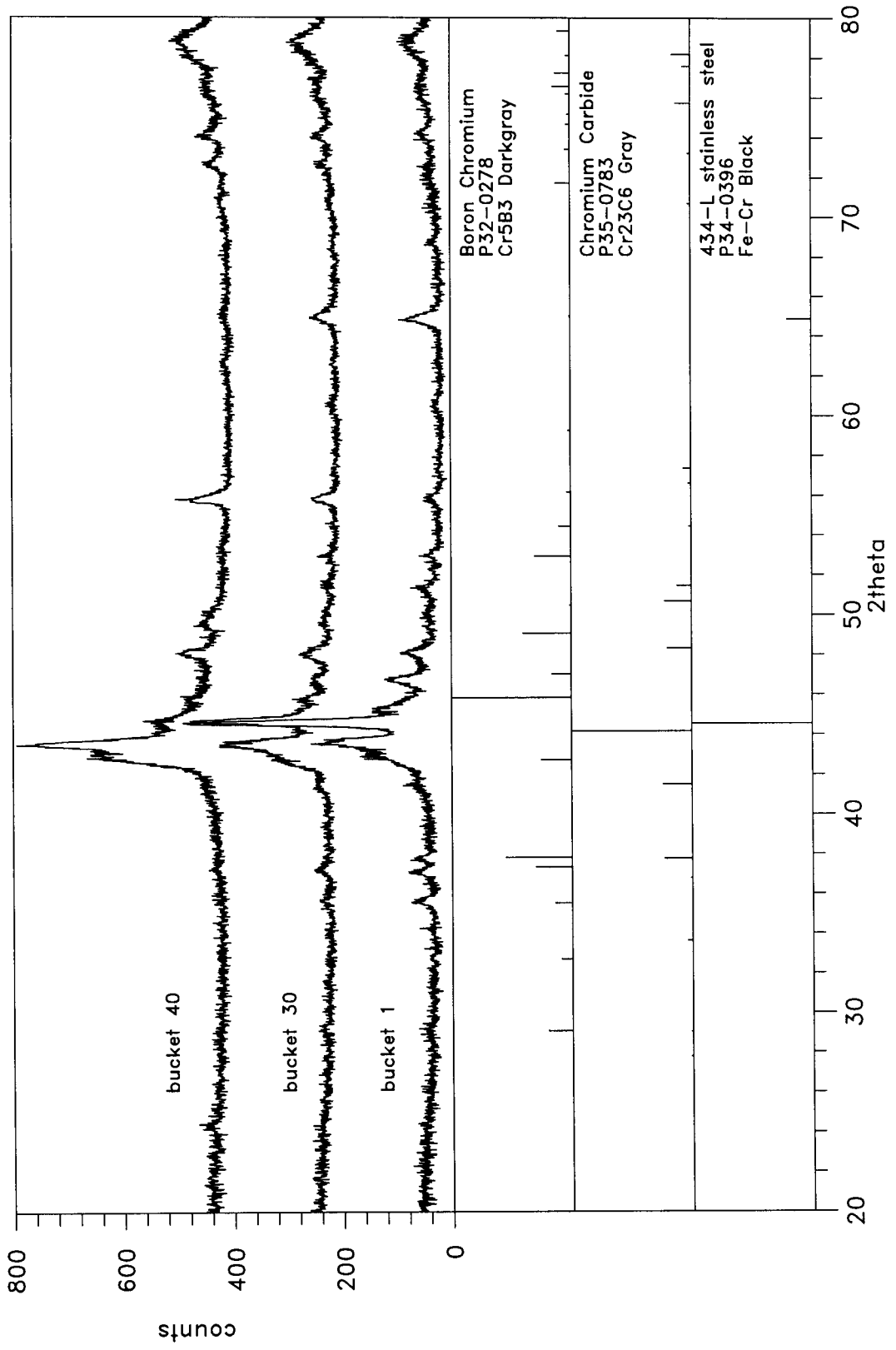
Figure 3: Comparison of XRD patterns for Fe-Cr-Mo-B-C powders "old" and "new"

(b) 05-263 old

(a) 06-015 new
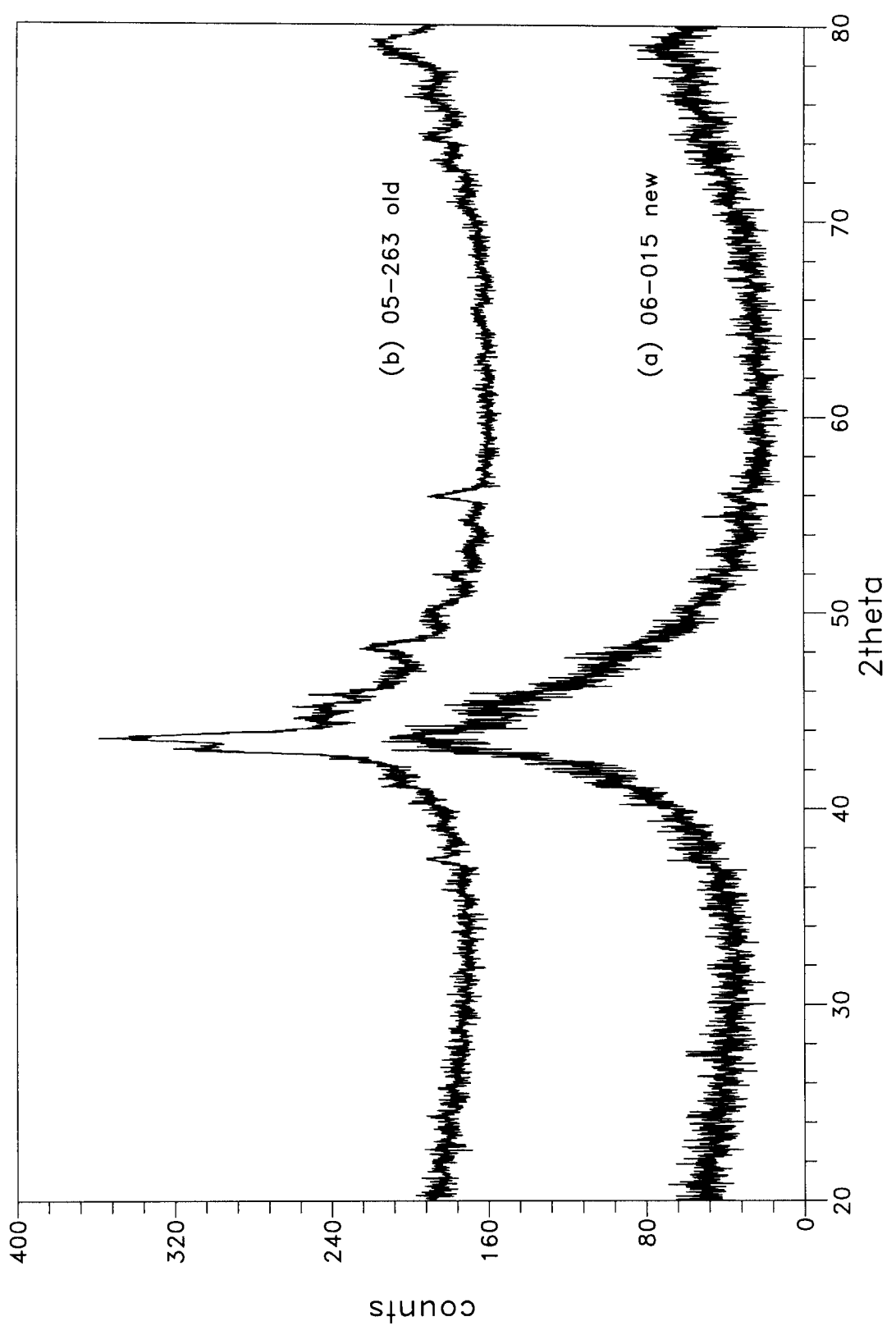
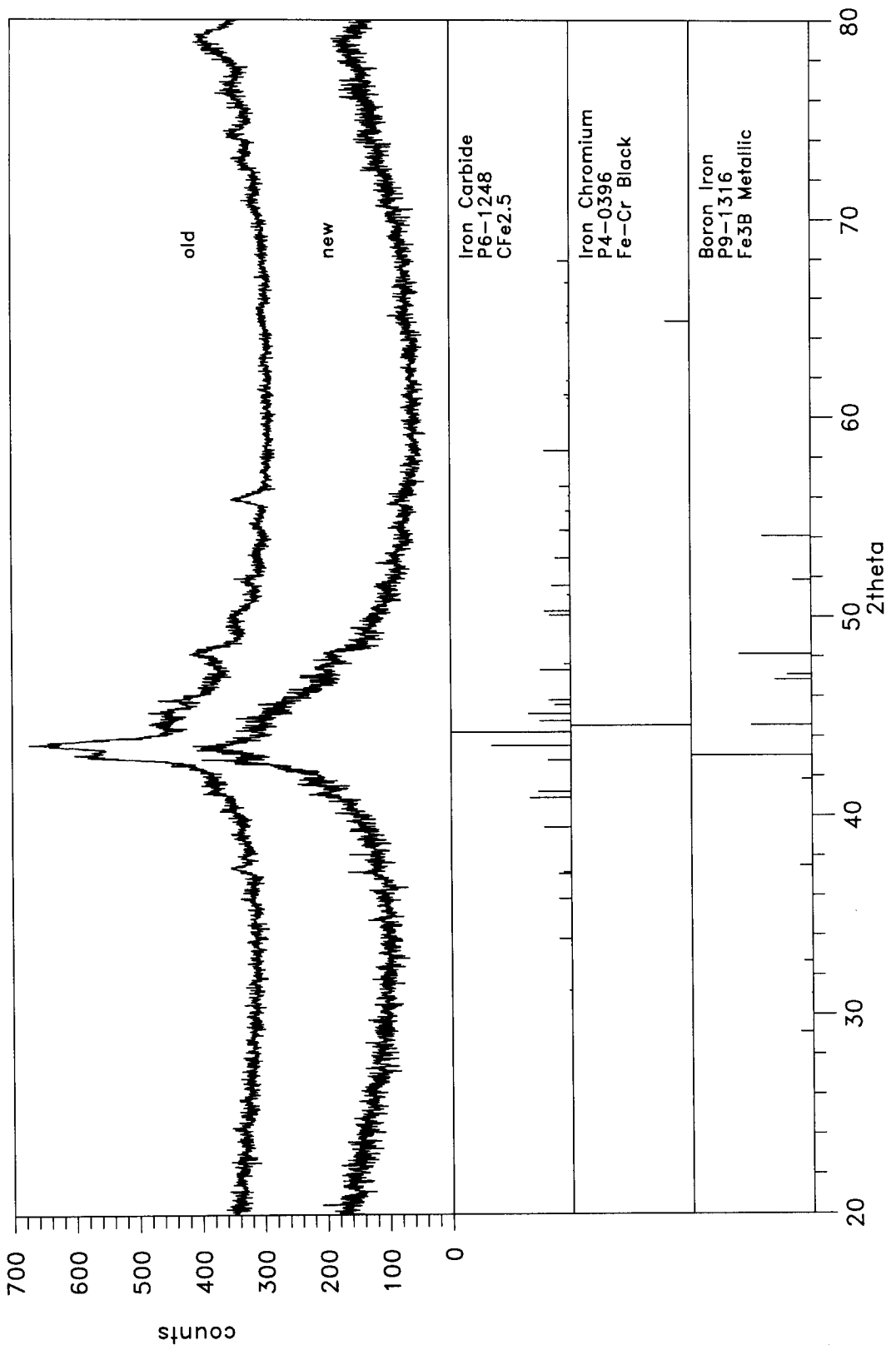Figure 4: XRD patterns for "old" and "new" powders along with the ICDD listings

Figure 5: XRD patterns for lot #06-015 SAM2X5 powders for different buckets
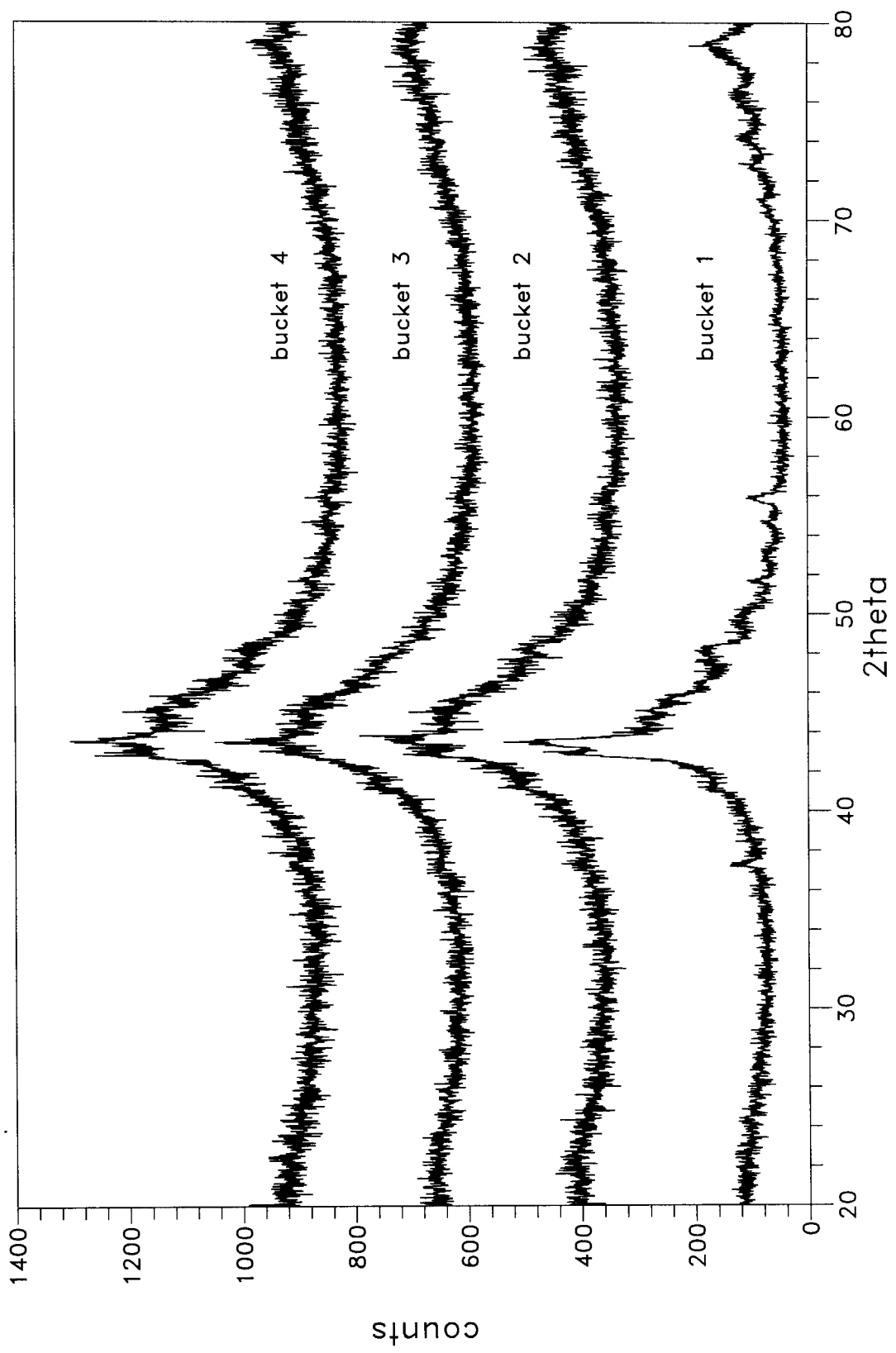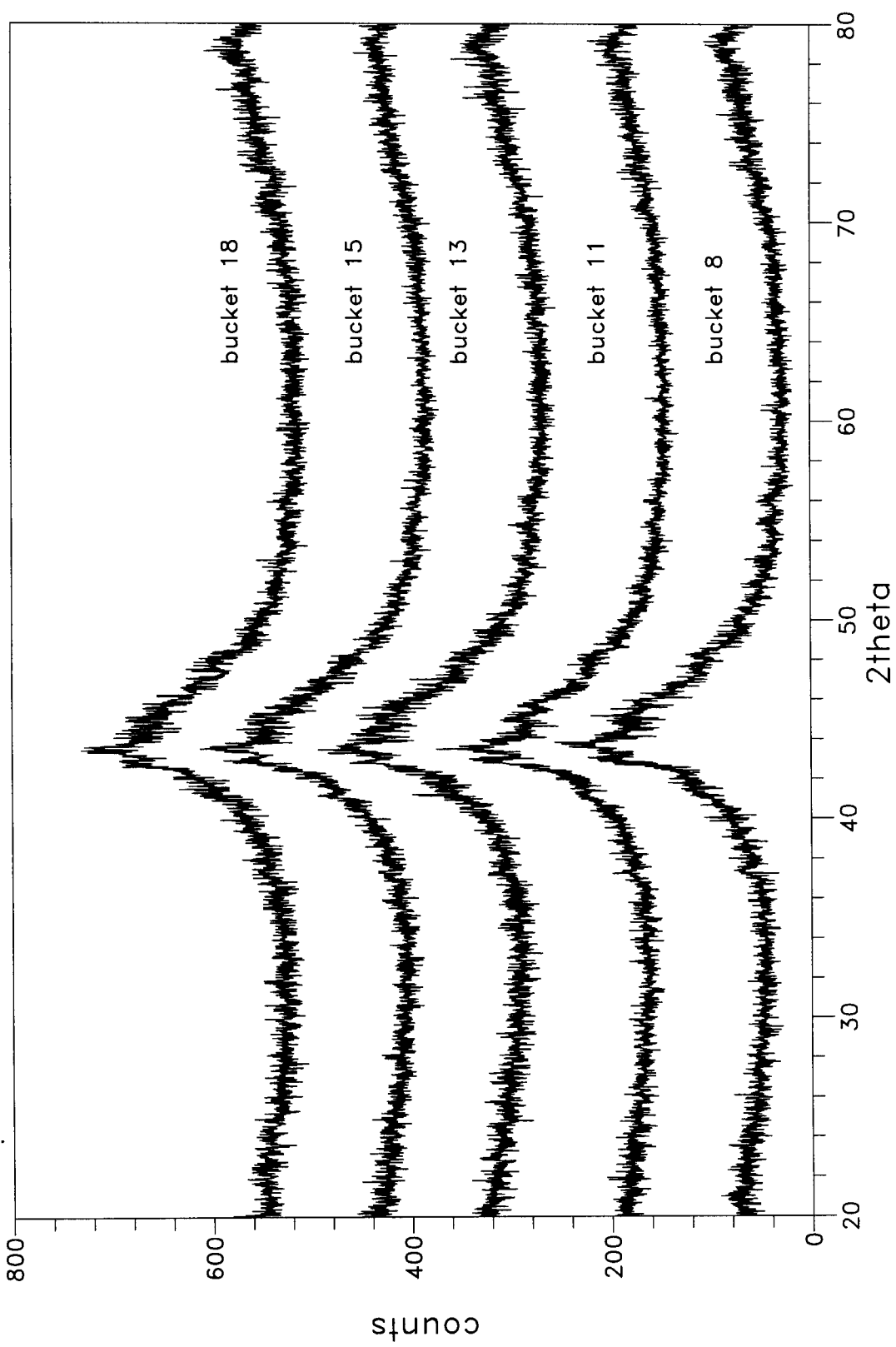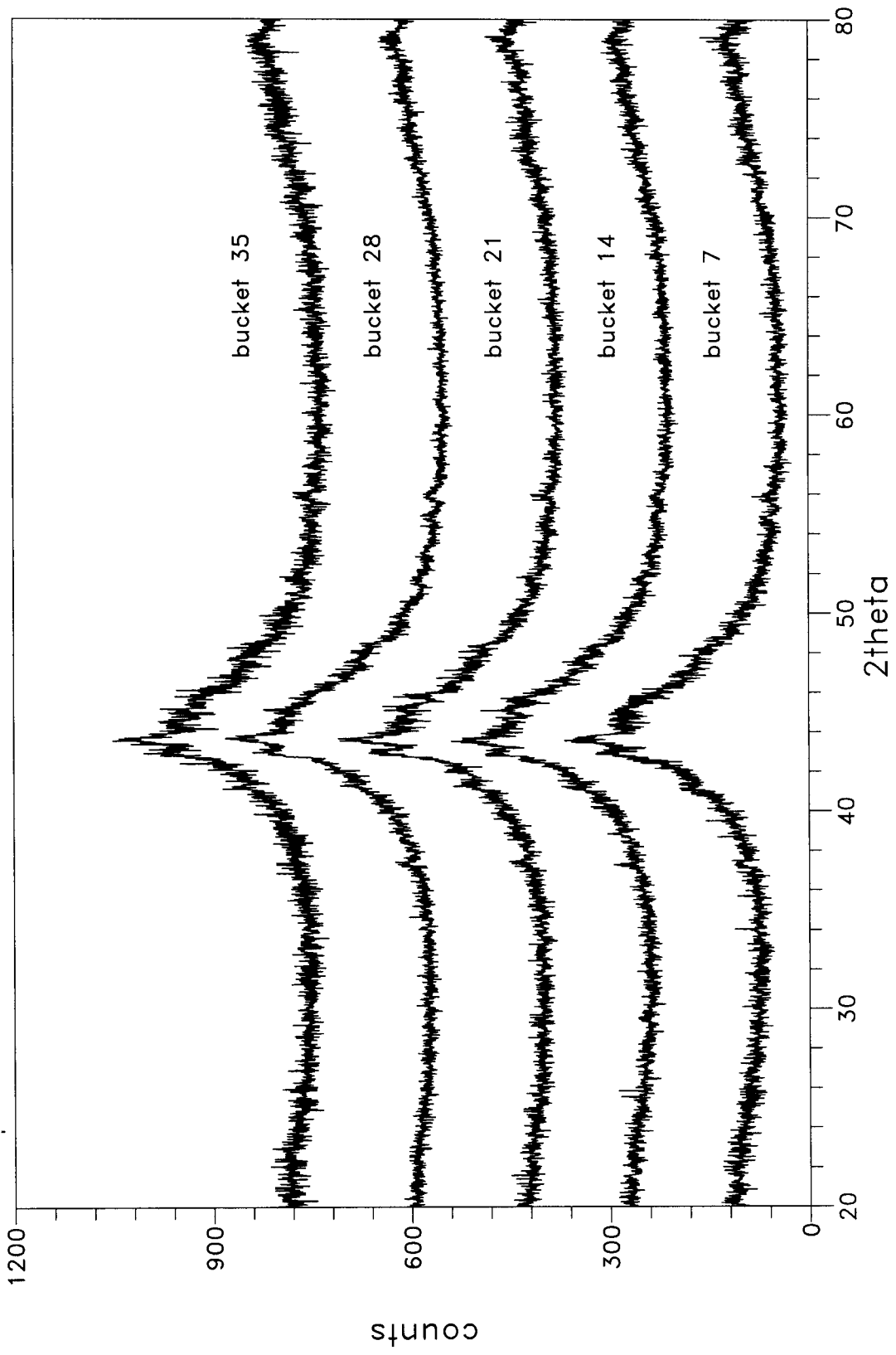
Figure 6: XRD patterns for lot #06-015 SAM2X5 powders for different buckets

Figure 7: XRD powder for lot #06-015 SAM2X5 powders from different buckets

bucket 35

bucket 28

bucket 21

bucket 14

bucket 7

counts

2theta

Figure 8: XRD pattern for lot #06-015 powder bucket 7 along with the ICDD listing
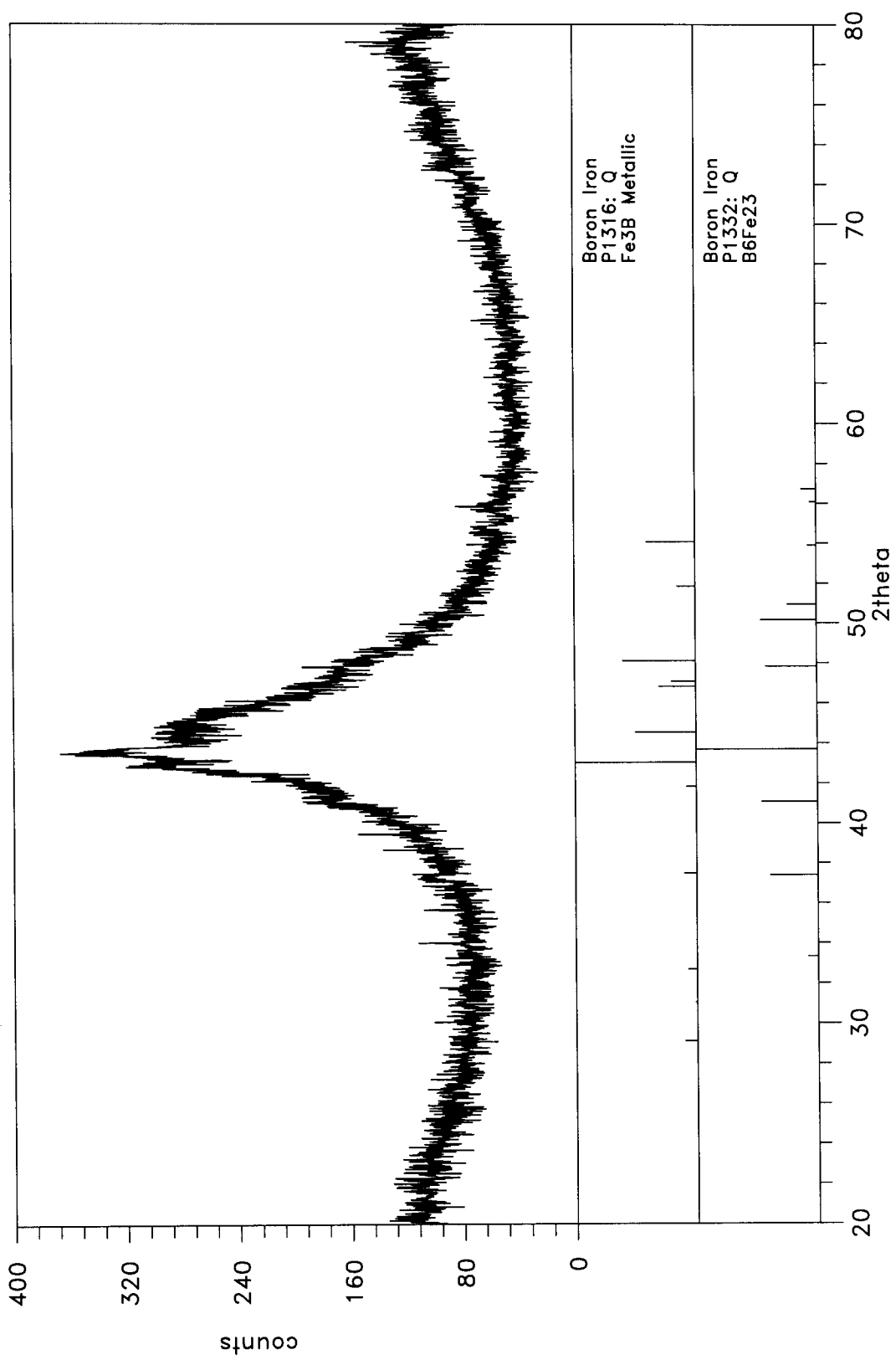
Figure 9: XRD pattern for lot #06-123 powders buckets 7, 9, 11, 13 and 15
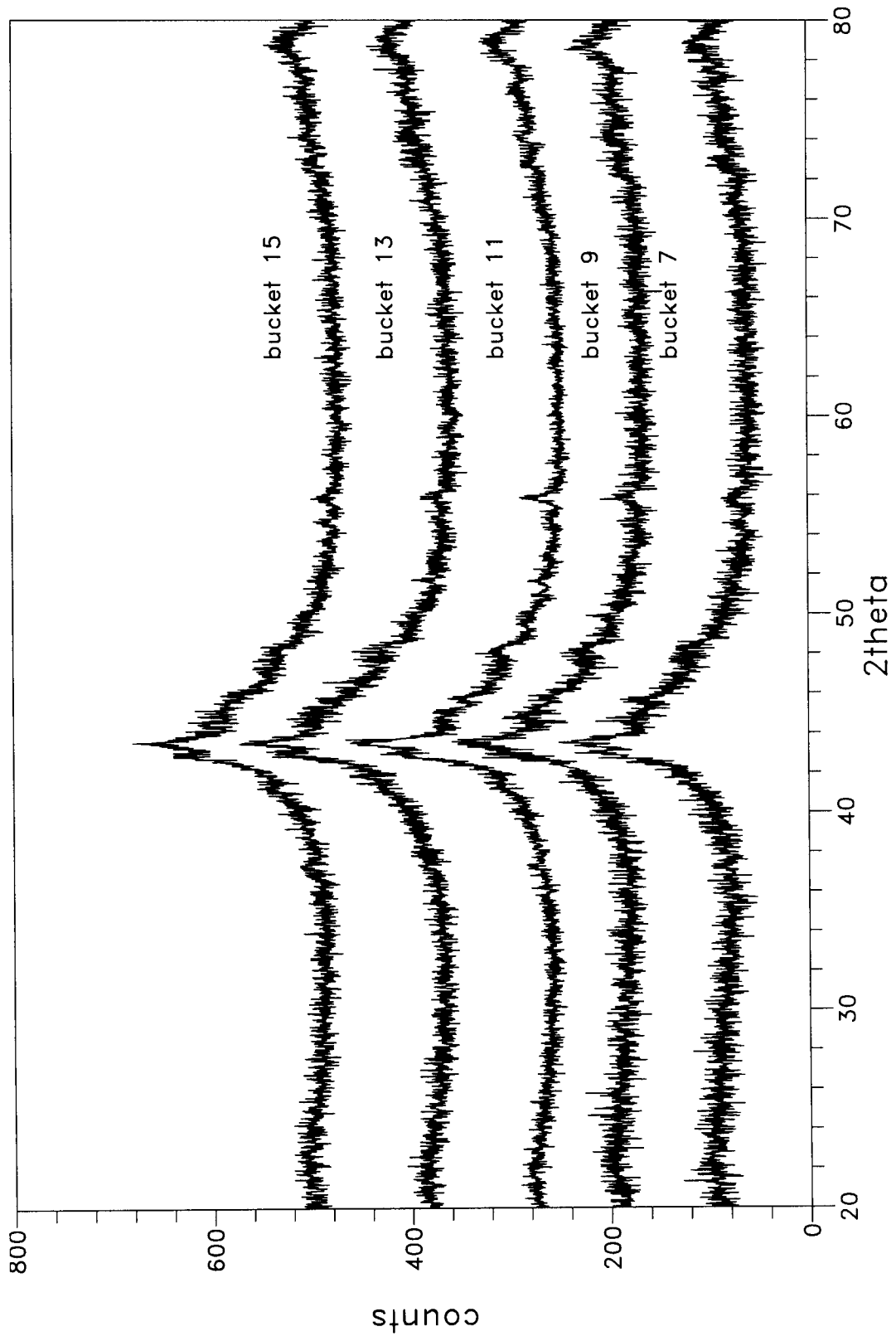
Figure 10: XRD of ribbons of C22 and 316C
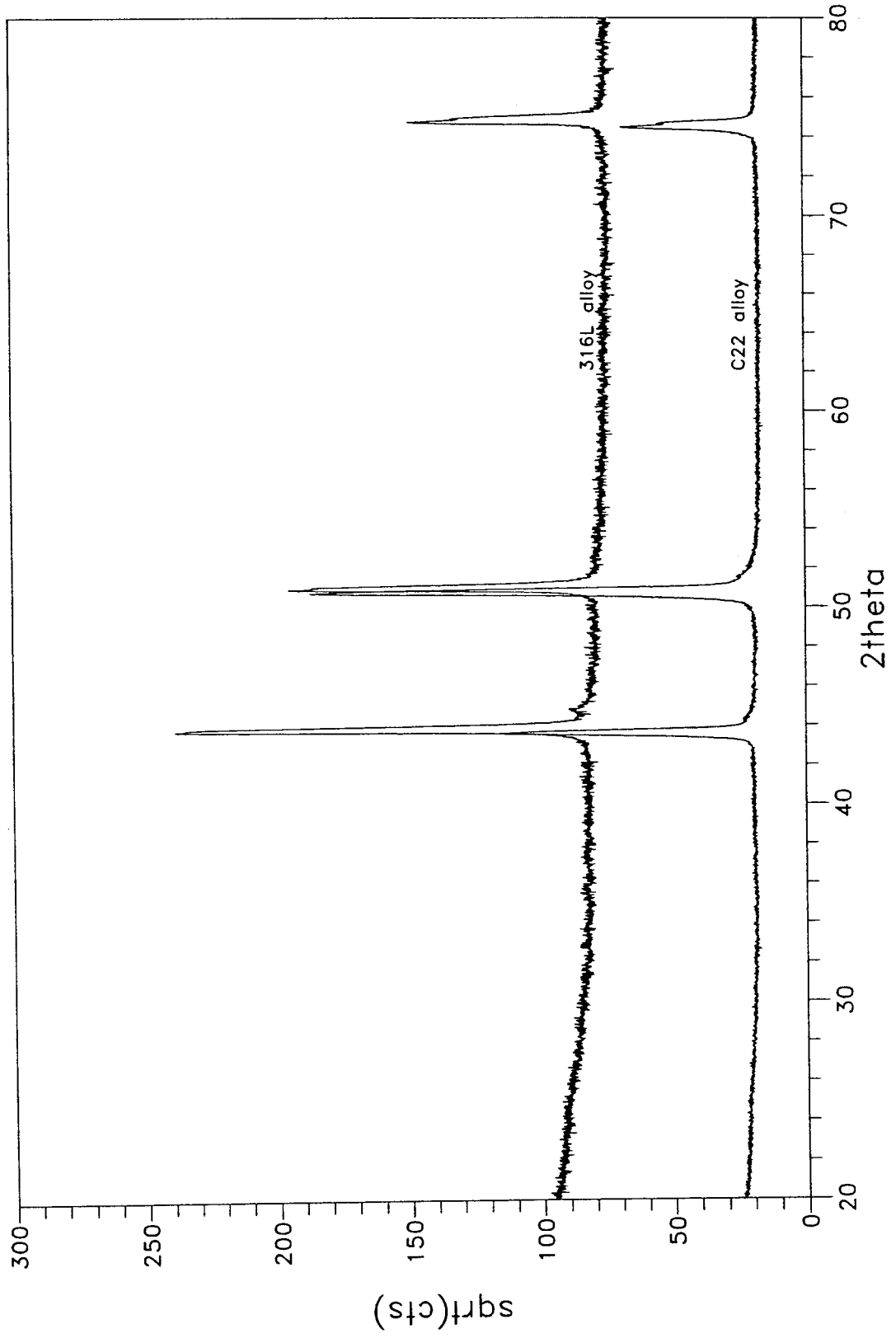
Figure 11: XRD patterns for the SAM2Xn, n is 1, 3, 5 and 7 ribbons
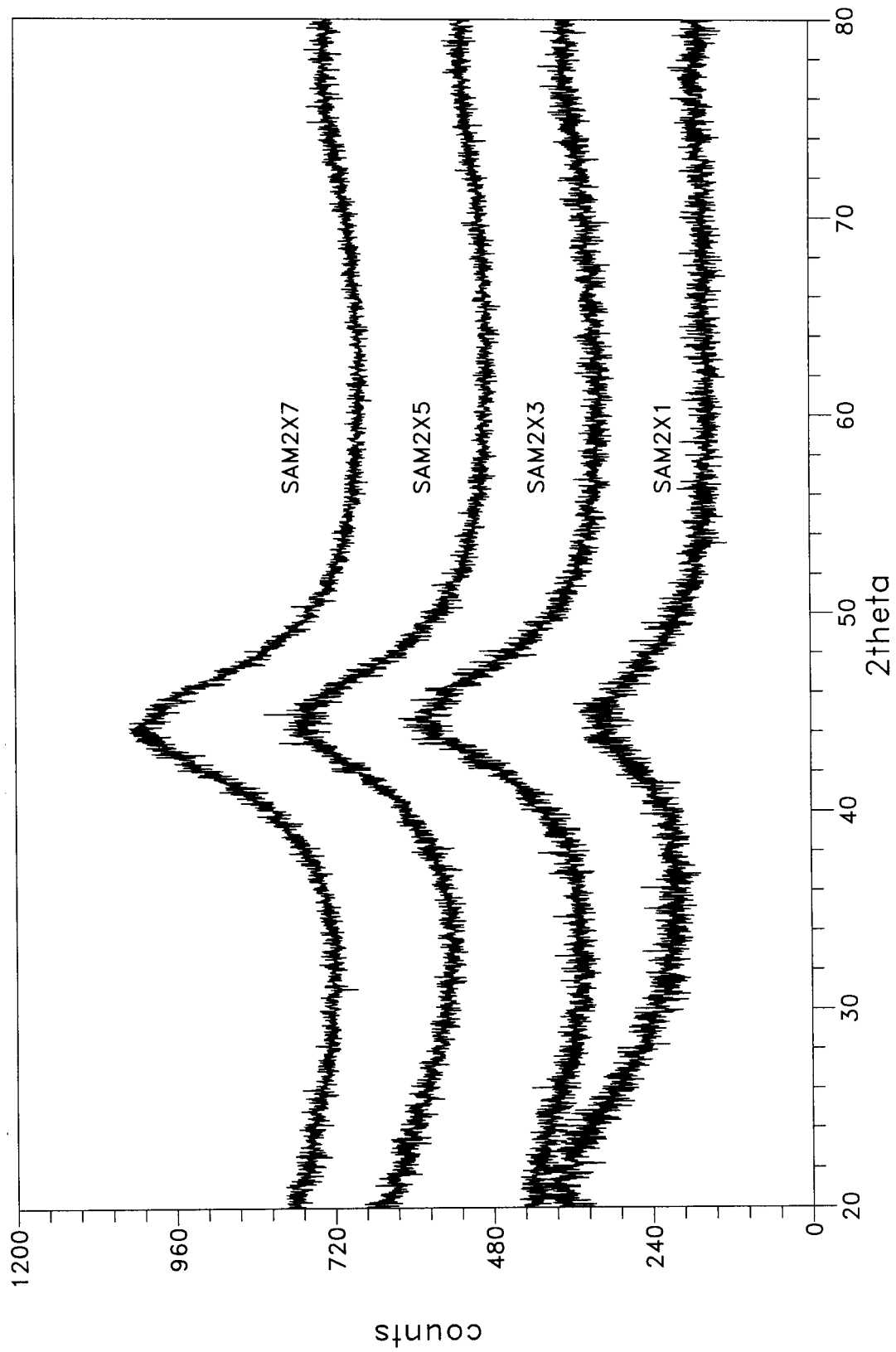
Figure 12: XRD patterns for the (e) SAM6, (f) SAM7, (g) SAM8 and (h) SAM40 ribbons
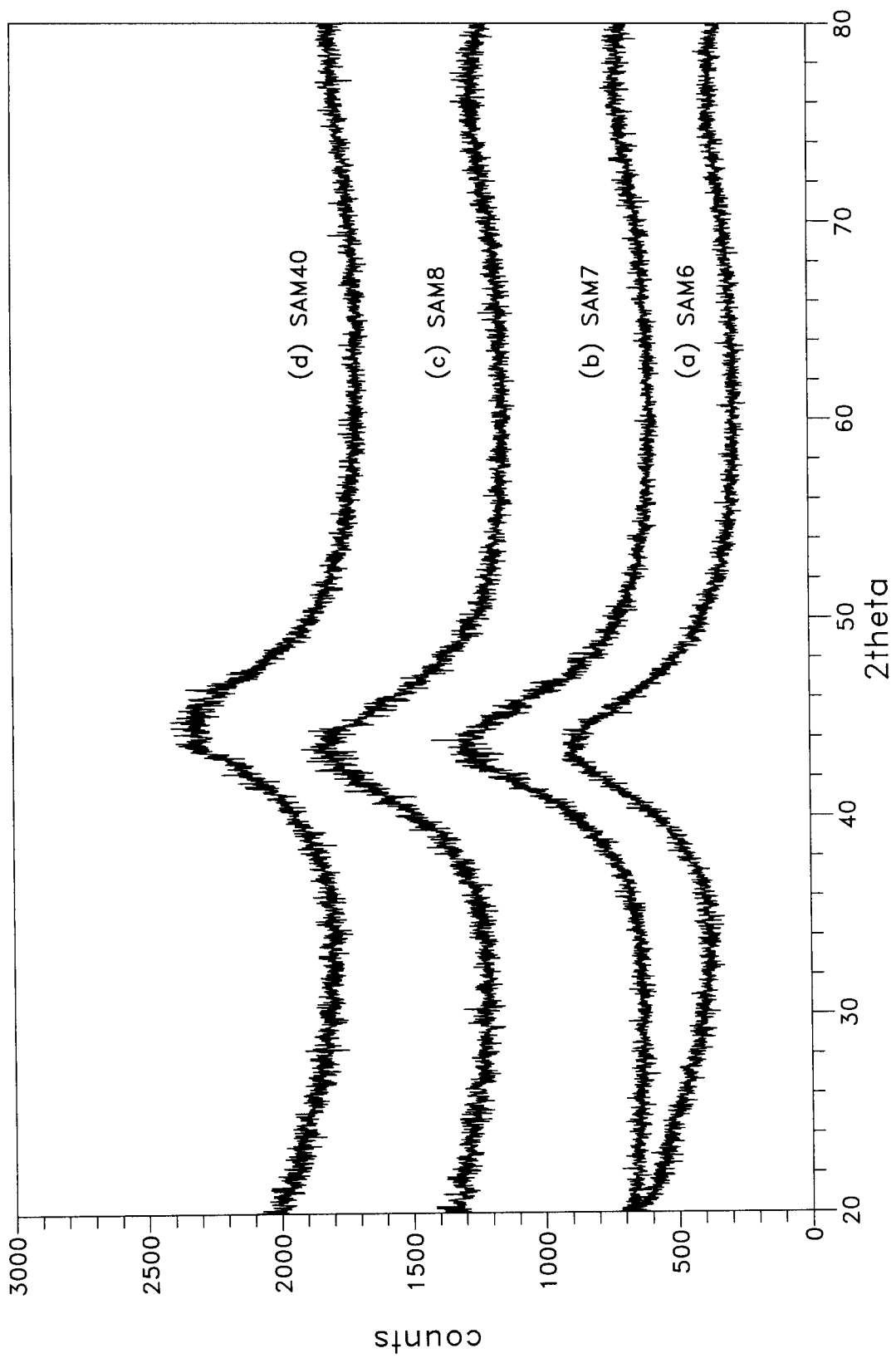
Figure 13: XRD of SAM1Xn, n=1, 3, 5 and 7 and SAM40 ribbons
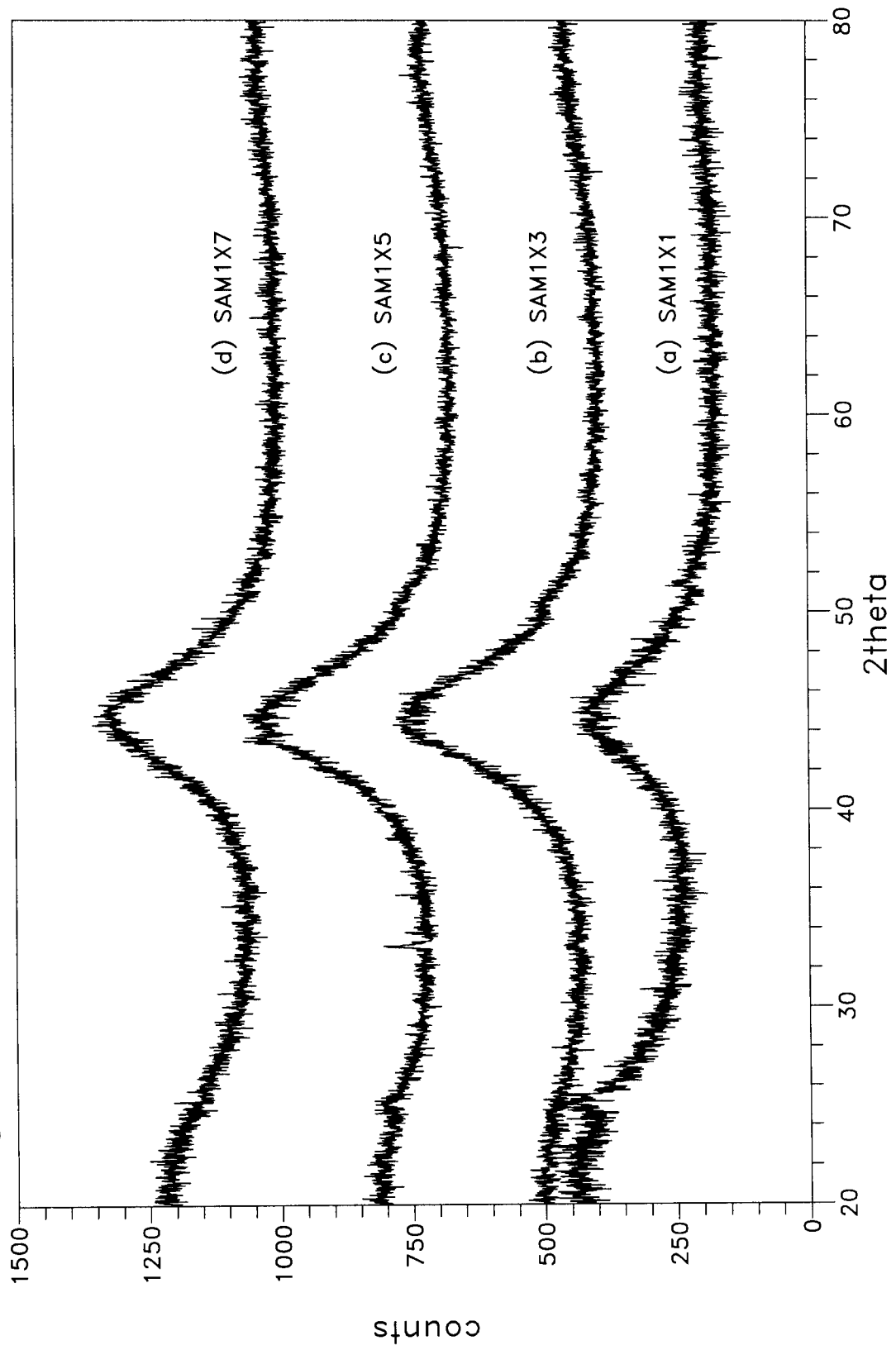
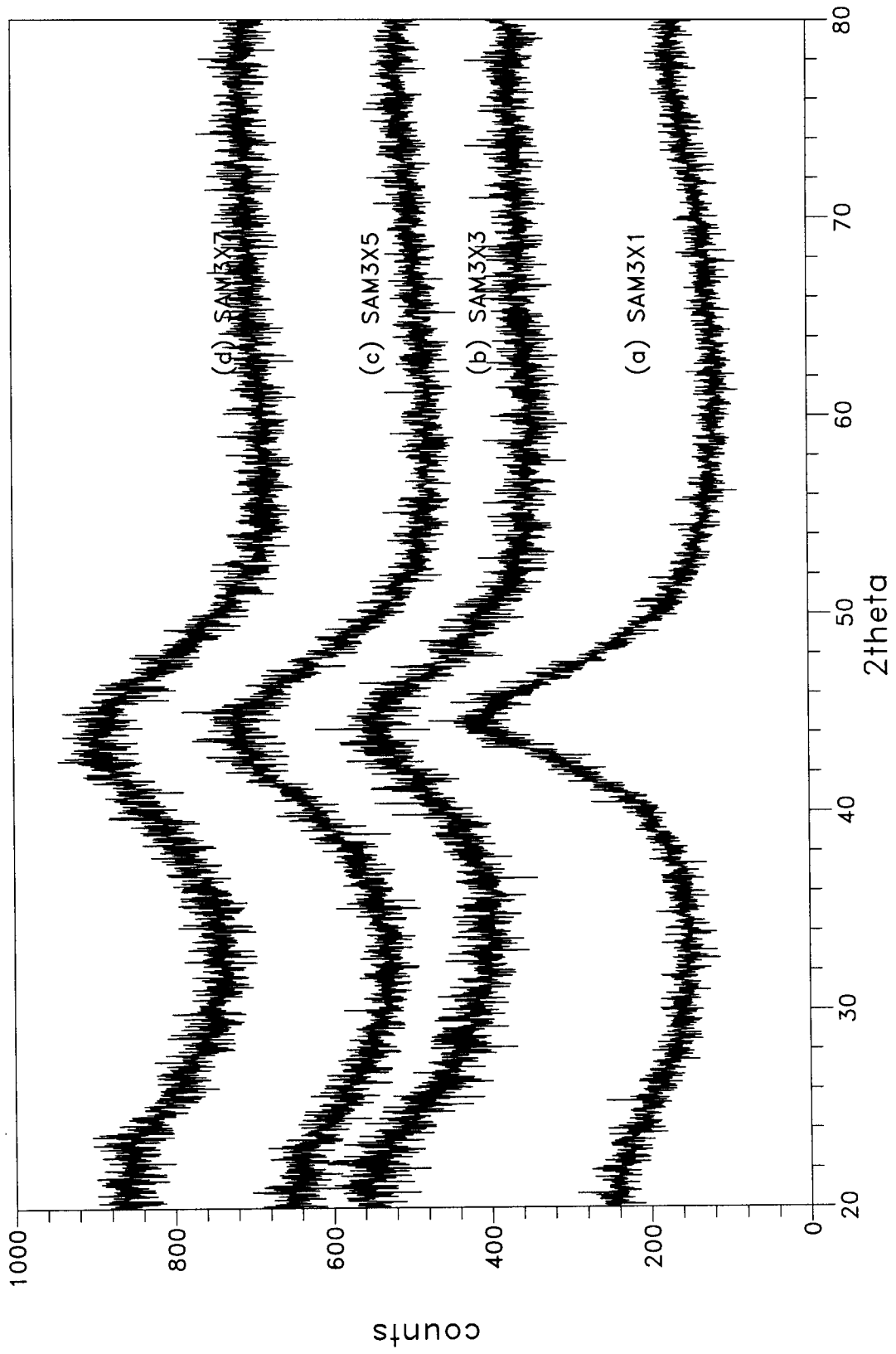Figure 14: XRD of SAM3Xn, n=1, 3, 5 and 7 and SAM40 ribbons

(d) SAM3X7

(c) SAM3X5

(b) SAM3X3

(a) SAM3X1

Figure 15: XRD of coatings (a) spalled SAM1651 and (b-e) SAM2X5 coatings
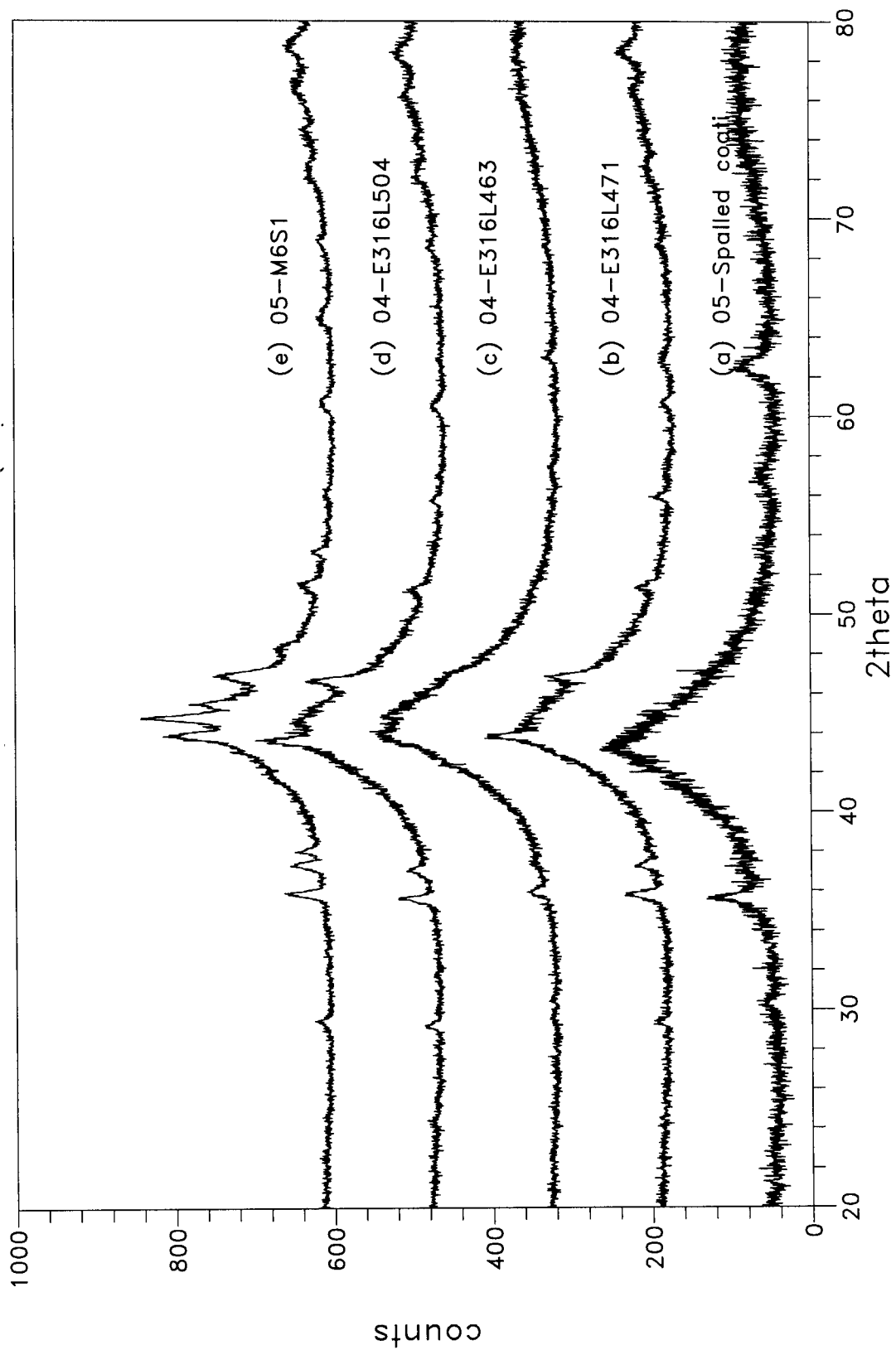
Figure 16: XRD of (b) and (d) coating along with the iron oxide ICDD listing
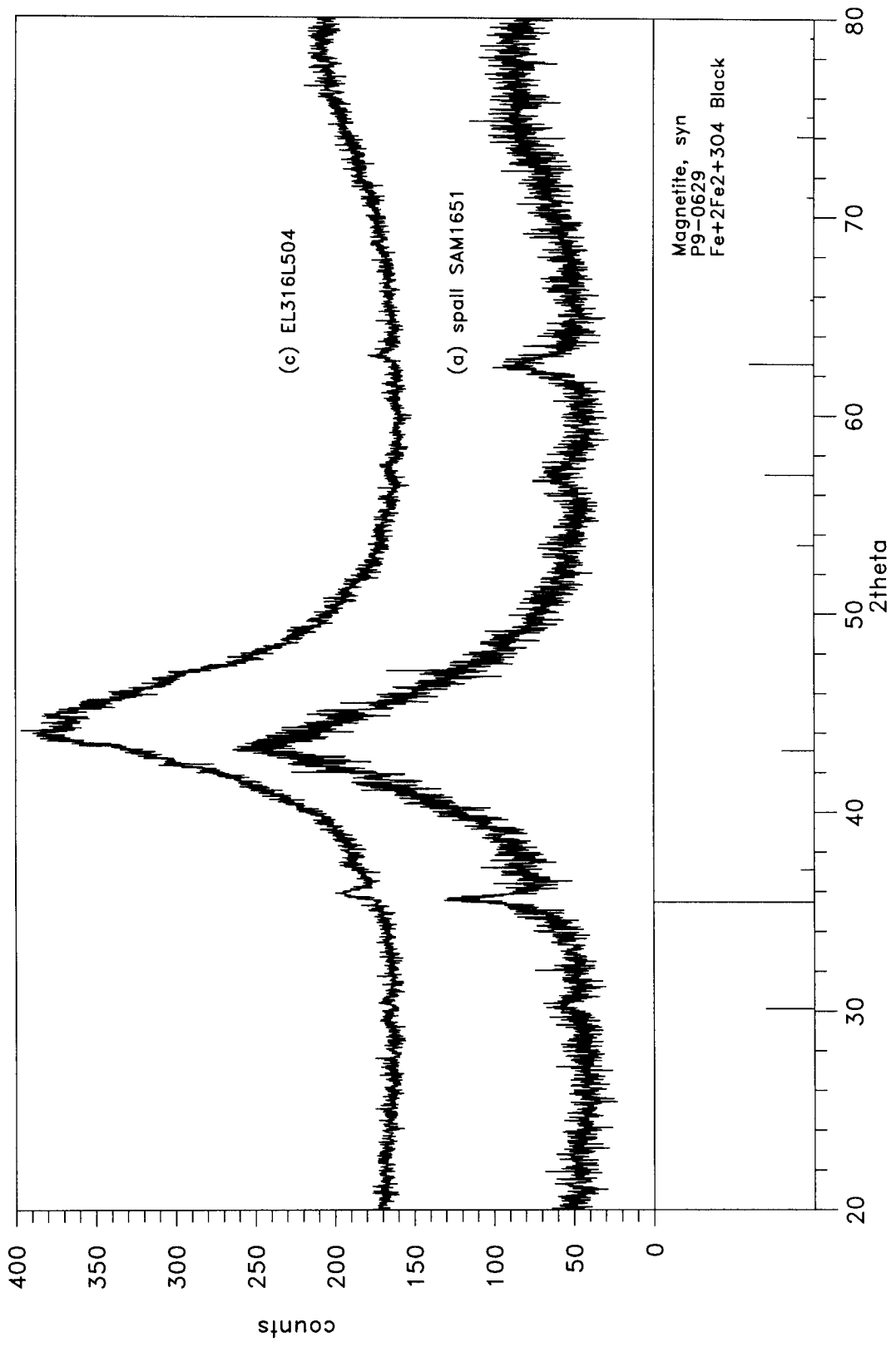
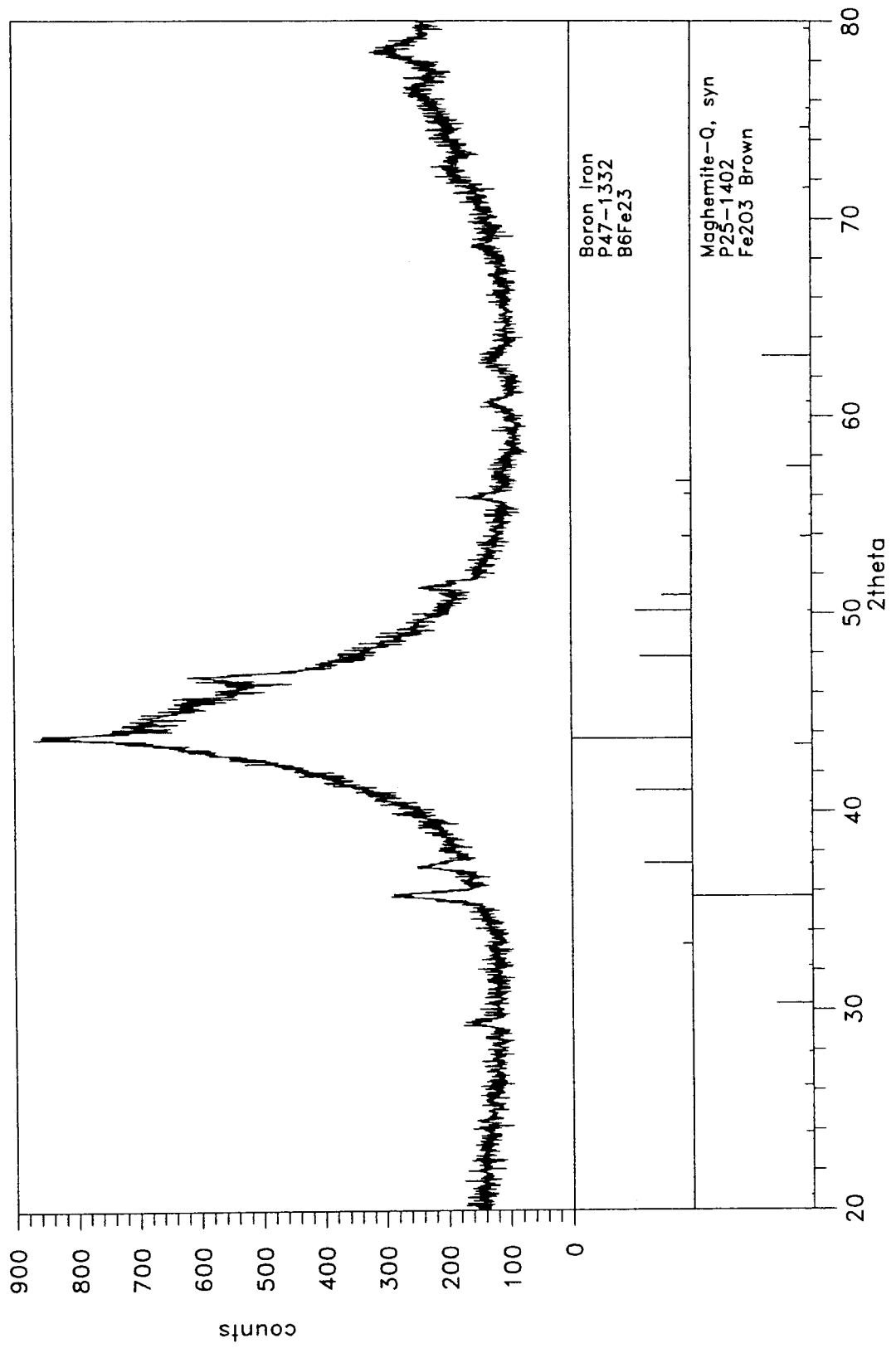Figure 17: XRD of (c) SAM2X5 coating along with the ICDD listing

Figure 18: XRD of SAM2X5 coatings labeled as PTI-A, PTI-B and PTI-C